Engineering Nanomolar Potent Protein-based Inhibitors for Papain-like Protease Guided by Residue Correlation Network

Ta I Hung[1,2#], Yun-Jung Hsieh[3,4#], Wei-Lin Lu[3], Kuen-Phon Wu[3,4*], and Chia-en A. Chang[1*]

1. Department of Chemistry, University of California, Riverside, United States
2. Department of Bioengineering, University of California, Riverside, United States
3. Institute of Biological Chemistry, Academia Sinica, Taiwan
4. Institute of Biochemical Sciences, National Taiwan University, Taiwan

# These authors contributed equally to this work

* Correspondences

Kuen-Phon Wu: kpwu@gate.sinica.edu.tw

Chie-en A. Chang: chiaenc@ucr.edu

Abstract

We developed a rational protocol with a minimal number of mutated residues to create highly potent and selective protein-based inhibitors. Guided by an interaction and dihedral correlation network of ubiquitin (Ub) and MERS coronaviral papain-like protease (PLpro) complex, our designed ubiquitin variant (UbV) with 3 mutated residues (A46F, K48E, and E64Y) resulted in a ~3,500-fold increase in functional inhibition as compared with the wild-type Ub (wtUb). Further optimization with C-terminal R74N and G75S mutations led to a K_D of 1.5 nM and IC_{50} of 9.7 nM and 27,000-fold and 5,500-fold increases in affinity and potency and selectivity, respectively, without destabilizing the UbV structure. This approach effectively designs tight binding inhibitors, which assists the development of therapeutics for COVID-19 and other coronaviruses.

Efficiently determining which residues of a protein to modify to increase the binding affinities between a protein-based inhibitor and the target protein is the key in protein drug development. Strategies that can accurately identify residues for protein engineering to increase protein–protein interaction (PPI) also have broad applications in therapeutics and cell-biology studies. In addition, utilizing a handful of mutated residues to achieve significantly enhanced PPI lowers the possibility of introducing unstable engineered proteins. However, the task is even more challenging because it requires highly integrated molecular modeling and experimental techniques to understand PPIs for rational protein design.

Ubiquitin (Ub) is a 76-residue small protein associated with post-translational modifications. It plays critical roles in numerous biological functions[1]. Ub canonically binds to its cascade E1-E2-E3 enzymes for ubiquitination and Ub chain formation to modify nearly half of the human proteome[2,3]. Conversely, deubiquitinase (DUB)[4] cleaves the covalent isopeptide bonds from the Ub chains or substrates to release Ub and substrates. Misregulation of these enzymes substantially affects cellular functions, hence leading to diseases such as cancers[5]. DUBs have been identified in several viral genomes as a tool interfering in the host antiviral defense. Papain-like protease (PLpro) of coronavirus (CoV) is classified as a Ub-specific protease type of viral DUB[6,7]. Studies show that PLpro alters the innate immune responses, which contributes to the rapid spread of CoVs (MERS, SARS-CoV, SARS-CoV-2) [8–12], thus causing pandemic deaths and decreasing the global economy[13].

PLpro of MERS and SARS-CoV-2 are crucial for viral replication via proteolytic cleavage of viral nonstructural proteins (NSPs). The PLpro domain resides in NSP3, which drives viral genome replication and subgenomic RNA synthesis.[14,15] PLpro can recognize and cleave the NSP1-2, NSP2-3 and NSP3-4 junctions after the amino acid sequence LXGG to yield functional viral proteins as well as perform deubiquitination and deISGylation.[11,12,16] Deubiquitination and deISGylation alter host signaling pathways critical for inducing cellular antiviral and pro-inflammatory innate immune responses and eventually suppresses the antiviral response.[16,17] Therefore, inhibition of PLpro simultaneously disrupts the viral replication and prevents PLpro from disrupting the innate immune response. With both properties, PLpro is an ideal antiviral drug target.

Although small molecule inhibitors achieve μM to sub-μM half maximal inhibitory concentration (IC_{50}) of the PLpro of SARS-CoV and CoV-2[12,16,18–20], engineering its natural substrate Ub as a protein-based inhibitor offers an alternative strategy to inhibit PLpro function. Importantly, wtUb exhibits high thermostability (T_m > 90˚C) and so is a great template for protein design. The protein drug also has potential advantages such as good binding specificity to PLpro and easy synthesis as compared with chemical compounds. Phage-display screened Ub variants (UbVs) against cognate enzymes including MERS PLpro demonstrated their feasibility in regulating the activities of E3 ligases and DUBs[21,22]. Computational results were used to rationally design a screening library for identifying tight binding regulator UbVs for USP7[23] and USP21[24]. However, the empirical screening remains expensive and time-consuming.

Here we present an integrated computational and experimental approach to design UbVs with 2 to 3 mutated residues to achieve 3500-fold inhibitory efficiency and binding affinity as compared with the wtUb to MERS PLpro and create protein-based inhibitors to inhibit the function of the viral protein (Table 1). MERS PLpro cleaves both K48 and K63-linked Ub chains,[6,11] and it has distinct inhibitor recognition specificity different from SARS-CoV and SARS-CoV-2.[25] Here we used non-covalent amino acid interaction networks of the Ub and MERS PLpro (Ub-PLpro) complex to guide the design of UbVs for increasing the UbV–PLpro binding affinity that inhibits the function of PLpro. The initial design began with 2-point mutations for cost-efficient experiments and for keeping an intact overall complex structure. Binding affinity K_D and IC_{50} measurement confirmed the inhibition of our designed dual-mutation UbVs and suggested additional UbVs. Integrating both experimental data and computation analysis re-informed the design to yield more UbVs for experiments (Fig. 1).

We first performed several 500-ns atomistic molecular dynamic (MD) simulations to model full protein flexibility for the wtUb–PLpro complex. By using combined side-chain dihedral correlation (Fig. S1A) and force distribution analyses (FDA)[26,27] (Fig. S2), we identified 4 highly correlated regions at the contact interfaces of Ub–PLpro: the hydrophobic core, alpha helix, C-terminal tail of Ub (named Ub-tail), and Zn binding region (Fig. 2). Next, we suggested highly interactive residues with strong correlation in the residue network as potential mutation residues in each region (Fig. 2 and see method in Fig. S1). Notably, existing studies showed that altering residues near the C-terminus of Ub hampered its biological function;[28–30]

therefore, we hypothesized that mutating our suggested residues in the Ub-tail could prevent the substrate from ubiquitination. MERS PLpro favors binding and cleaving K48 and K63-linked Ub chains[6,11], which implies that residues near the conjugation points interact with PLpro frequently. Of note, K48 and K63 are in the hydrophobic core and Zn binding region, respectively. Mutating residues in the dense interactive spots may easily hamper PPI, which also offers potential in strengthening their interactions. Because the Zn binding and Ub-tail regions are more flexible, we began with modifying A46 and K48 in the hydrophobic core and V70 and R42 in the helix region. We considered side-chain proximity between a UbV and PLpro to utilize unused space or enhance charge-charge attraction to design mutations. Coincidentally, these mutated residues were also reported in existing UbVs[31].

To predict the intermolecular attractions between each UbV-PLpro, we used molecular mechanics Poisson-Boltzmann surface area (MM/PBSA) and local structural analysis to evaluate PPI energy (Fig. S3) and investigate the local attraction (Fig. S4), respectively. Variants with A46 and K48 mutation led to better UbV–PLpro attractions. However, the K48E-V70E variant could not yield good van der Waal (vdW) interactions and modifying R42 to the oppositely charged residue R42D yielded poor predicted UbV–PLpro interaction energies (Table S1 and Fig. S4). The results suggested that mutating R42 or V70 may not lead to tight binding events. Hence, we first focused on the variants altering A46 and K48. Additionally, for every designed UbV with predicted stronger UbV–PLpro attractions than that of wtUb (Table S1), we also performed PPI Gaussian-accelerated MD (PPI-GaMD) in an explicit solvent model to examine their binding residence time, with protein flexibility and solvent effects also considered[32] (Fig. S5). Because PPI-GaMD applied boost potential to enhance conformational sampling, the residence time cannot be compared directly with the binding affinity or dissociation rate constant (k_{off}). Nevertheless, the dissociation time for these UbVs was all longer than that of the wtUb, which suggests that these variants should serve as tighter binders than wtUb.

Next, we evaluated the UbV-dependent inhibitory efficiencies for MERS PLpro by using sensitive fluorescent polarization (FP) to monitor the dynamics of fluorescein conjugated to the C-terminus of ISG15 (Fig. S7). We examined the designed 4 UbVs with dual mutations in positions A46F and K48 (E, S, I and L) as well as 2 single-mutation UbVs, A46F and K48E.

The designed UbVs all bound tightly to PLpro (K_D in Table 1) and efficiently inhibited the enzyme function with reduced IC_{50} (Fig. 3A). In comparison to wtUb, substitution of A46 in the hydrophobic core by a non-polar residue PHE successfully formed stronger vdW attractions with nearby residues of PLpro (Fig 4A and Table S1). For example, A46F induced local conformational arrangements and recruited Y208 and Y223 in PLpro to form pi-pi interactions and R233 in PLpro to form pi-cation attractions (Fig 4A). The polarity of K48 in wtUb significantly affected both the local interactions and network correlation due to the large repulsive force to the surrounding K204 of PLpro. Mutation of K48 to nonpolar or negatively charged residues such as LEU or GLU should increase the attractive forces with the K204 (Fig. 4A). Notably, the single-point mutations A46F and K48E could achieve an IC_{50} 1.6 and 3.9 μM, respectively, as compared with wtUb (52.9 μM). The 46-48 mutants further elevated the inhibition to IC_{50} ~0.2 μM (Table 1), approximately 250-fold as compared with wtUb. We found a synergistic effect by A46F and K48E (or K48L/K48S/K48I) toward the interactions of PLpro and UbV (Fig. 3E).

We demonstrated that mutating two residues in the hydrophobic core is an effective strategy for inhibitor design, so we further added more mutated residues from our suggested list (Fig. 2). We chose A46F-K48E (termed UbV2), which exhibits good IC_{50} and K_D, and added one mutated residue, E64Y, from the Zn binding region. Because MERS PLpro explicitly recognizes K63-linked Ub chains, and our residue network shows a strong correlation around S65 (Fig. S1), we conjectured that modifying the nearby residue E64 may contribute to both binding strength and specificity. Experimental measurements for A46F-K48E-E64Y (termed UbV3) showed remarkable binding specificity and inhibition to PLpro, with an IC_{50} of 15 nM, significantly agreeing with the strongest computed binding energy (Table 1). Both the root mean square fluctuation (RMSF) and dihedral entropies of the protein (Fig. S6) were reduced as compared with that of UbV2, so the Zn binding region was largely stabilized in the UbV3–PLpro complex (Fig. 4B). The stability prediction also agrees with our experiments of UbV3 yielding high thermostability (Fig. S10). In addition to impressive functional inhibition, UbV3 bound highly specifically to MERS PLpro (Fig. S11), which is also an essential attribute for a good inhibitor.

We next altered two residues, R75 and G75 of the Ub-tail region from our non-covalent network, which also serve a role in preventing cells from utilizing the UbVs. New sets of 74 and 75 mutations were added to our dual UbVs (Table 1), and the 4-point mutation A46F-K48E-R74N-G75S (termed UbV4) yielded a reduced IC_{50} of 110 nM. Therefore, we further included E64Y to UbV4 to use all 3 highly correlated regions and the designed 5-point mutant UbV5, resulting in an IC_{50} of 9.7 nM (5,500-fold of wtUb) and K_D of 1.5 nM (Table 1). Our UbV3 and UbV5 exhibit great inhibition equivalent to the reported variants for MERS PLpro[31]. They also preserve the thermostability shown by far-UV circular dichroism. The reported variants with 15 mutated residues revealed denatured states at 80 ˚C[23] , which is significantly less thermostable than our UbVs (Fig S10). Mutating too many residues in Ub easily brings stability issues. Our work demonstrates the advantage and efficacy of modifying only a few residues of a protein template for protein-based inhibitors.

In this study, we established a novel approach to modify a minimum of 2 to 3 residues within the correlation network in the Ub–PLpro interface to enhance PPI and achieve 250- to 3,500-fold reduction of MERS PLpro activity. A combination of 5 mutated residues selected from the hydrophobic core, zinc finger region and the Ub-tail resulted in a 5,500-fold (IC_{50} = 9.7 nM) reduction in PLpro function and a 27,000-fold enhancement in UbV–PLpro complex affinity. Our design platform computationally examines a correlation network of protein sidechains and local pair-wise forces to efficiently design UbVs for experiments. Integrating experimental measurements and further structural analysis using MD simulations and post-analysis iteratively re-informs new design. The approach is transformative for identifying key mutation sites and specific residues to guide rational design with high efficiency for many Ub-bound DUBs and proteins[33,34], including SARS-CoV-2. In contrast to producing variant-specific antibodies/vaccines for diverse spike proteins, tight and specific UbV inhibitors for the PLpro-CoV2 can provide a prominent solution to retard viral replication and rescue the antiviral immune response simultaneously. Our platform is also generalized and can be applied to other protein templates for engineering tightly bound variants for various applications.

Acknowledgments

This study was supported by the US National Institutes of Health (GM-109045), the US National Science Foundation (MCB-1350401 to C.C), and an Academia Sinica (Taipei,

Taiwan) Career Development Award (AS-CDA-110-L03 to K.P.W.). We appreciate the technical and instrumental support from the Academia Sinica (AS) Biophysics Core Facility (AS-CFII-111-201) and the Biophysics Instrumentation Laboratory, Institute of Biological Chemistry, Academia Sinica

Ubiquitin and variants	Binding Energy (kcal/mol)	Dissociation Time (ns)	IC_{50}	K_D	PLpro selectivity*	
					MERS-CoV	SARS-CoV-2
w.t Ub	-41.95 ± 2.56	32	52.91 ± 6.98 μM	40.75 ± 3.82 μM	-	-
A46F	-48.25 ± 1.09	67.5	1.64 ± 0.03 μM	2.74 ± 0.29 μM	+++	-
K48E	-49.52 ± 2.56	75	3.94 ± 0.42 μM	5.15 ± 0.71 μM	++	-
E64Y	-42.00 ± 1.49	68	0.29 ± 0.03 μM	0.46 ± 0.04 μM	++++	-
A46F-K48E **(UbV2)**	-50.54 ± 2.35	207	0.20 ± 0.00 μM	0.22 ± 0.03 μM	+++++	-
A46F-K48L	-49.03 ± 2.33	200	0.23 ± 0.01 μM	N/A	N/A	N/A
A46F-K48S	-47.13 ± 2.84	N/A	0.18 ± 0.01 μM	N/A	N/A	N/A
A46F-K48E-G75R	-45.24 ± 1.48	40	9.74 ± 0.15 μM	11.41 ± 1.26 μM	N/A	N/A
A46F-K48I	N/A	N/A	0.49 ± 0.04 μM	N/A	N/A	N/A
A46F-K48E-E64Y **(UbV3)**	-53.77 ± 1.37	>250	14.84 ± 1.44 nM	2.77 nM	+++++	-
A46F-K48E-R74N-G75S **(UbV4)**	-50.18 ± 0.88	65	0.11 ± 0.01 μM	0.15 ± 0.02 μM	+++++	-
A46F-K48L-R74N-G75S	-46.49 ± 0.98	>250	0.13 ± 0.01 μM	0.14 ± 0.02 μM	N/A	N/A
A46F-K48E-E64Y-R74N-G75S **(UbV5)**	-50.81 ± 3.25	88	9.71 ± 0.74 nM	1.48 nM	+++++	-
ME.2**	-47.98 ± 1.72	>250	15.62 ± 2.54 nM	N/A	+++++	-
ME.4**	N/A	N/A	28.57 ± 1.94 nM	N/A	+++++	-

Table 1. Computational and experimental evaluation of binding affinity between MERS-CoV-PLpro and UbVs.

* One "+" indicates 0-20% reduction of PLpro activity compared to UbV-free conditions.

** ME.2 and ME.4 were previous UbVs[31] introducing 15 mutation sites. The PLpro selectivity for ME.2 and ME.4 UbVs were extracted from published work[31].

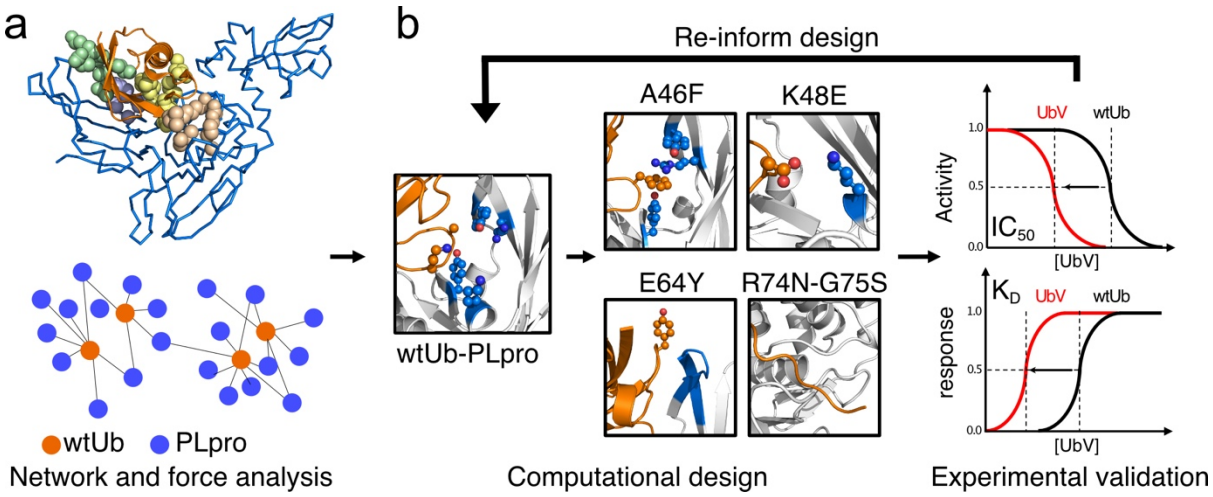

Figure 1. Workflow of rational design of ubiquitin (Ub) variants. **(a)** Molecular modeling with molecular dynamics (MD) simulations and post-analysis to reveal highly correlated regions between the interface of PLpro (presented marine trace) and Ub (orange). **(b)** Integrated computational and experimental design, validation, and interpretation.

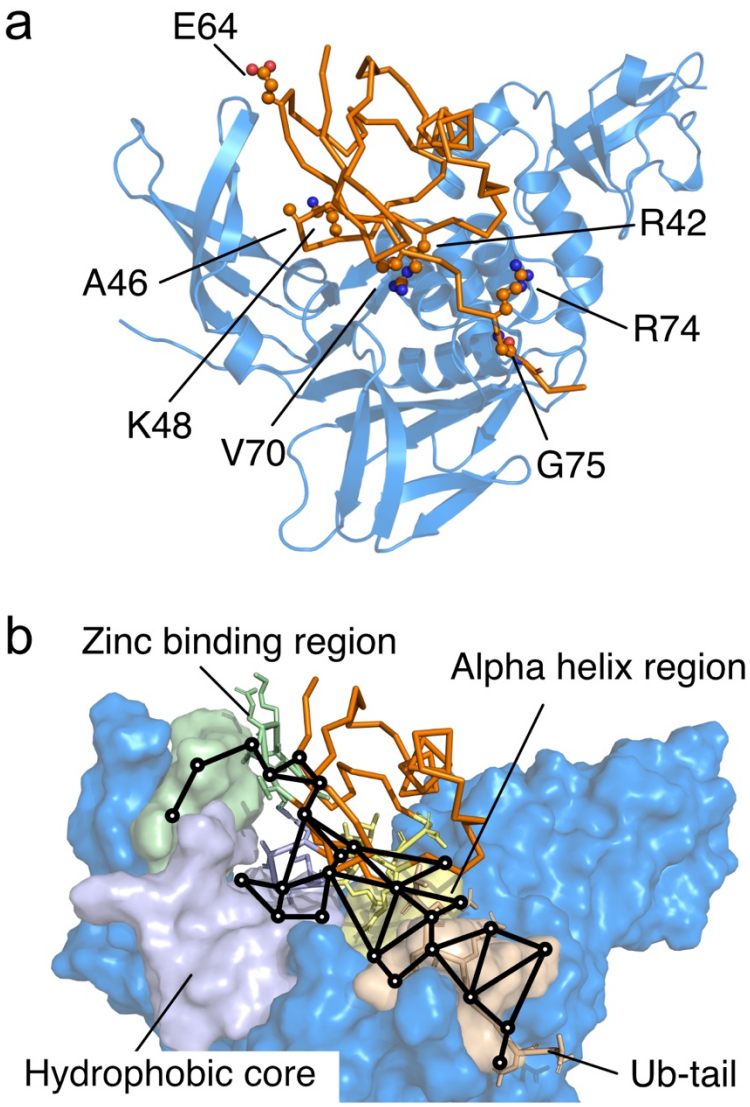

Figure 2. Highly correlated regions between Ub and MERS-CoV PLpro. **(a)** Suggested potential mutation residues based on interaction networks: R42, A46, K48, E64, V70, R74, and G75. Color-coded regions: Ubiquitin (Ub, orange), PLpro (marine), Zn binding region (palegreen), Hydrophobic core (lightblue), Alpha helix region (paleyellow) and Ub-tail (wheat). Note that R42 and V70 were not considered in further Ub variant (UbV) designs and experiments after computational prediction. **(b)** Computed dihedral correlation network showing how mutation leads to conformation changes at distal regions.

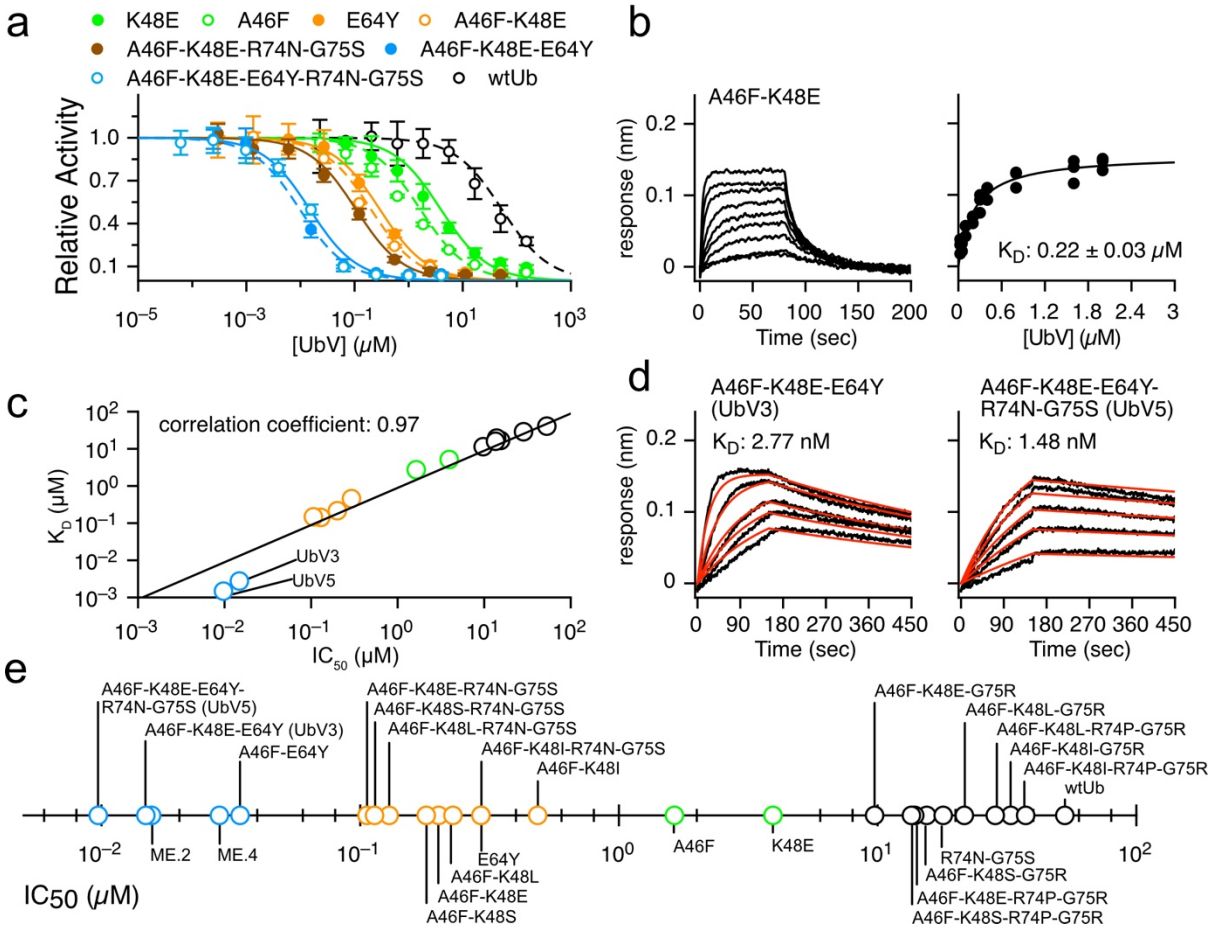

Figure 3. The inhibitory IC_{50} and affinity constants of UbVs. **(a)** IC_{50} curves of selected 7 UbVs and wild-type Ub (wtUb) show PLpro activity progressively inhibited from 2- to 5-point mutations. **(b)** BLI sensorgram and fitting curve of UbV2 show K_D of 0.22 μM. **(c)** The measured IC_{50} and K_D values are highly correlated. **(d)** BLI sensorgram of tight binders UbV3 and UbV4. (e) Experimentally measured IC_{50} of 26 UbVs are summarized in a logarithmic scale, with black, green, orange and blue circles indicating weak, medium, strong and very strong inhibitors, respectively.

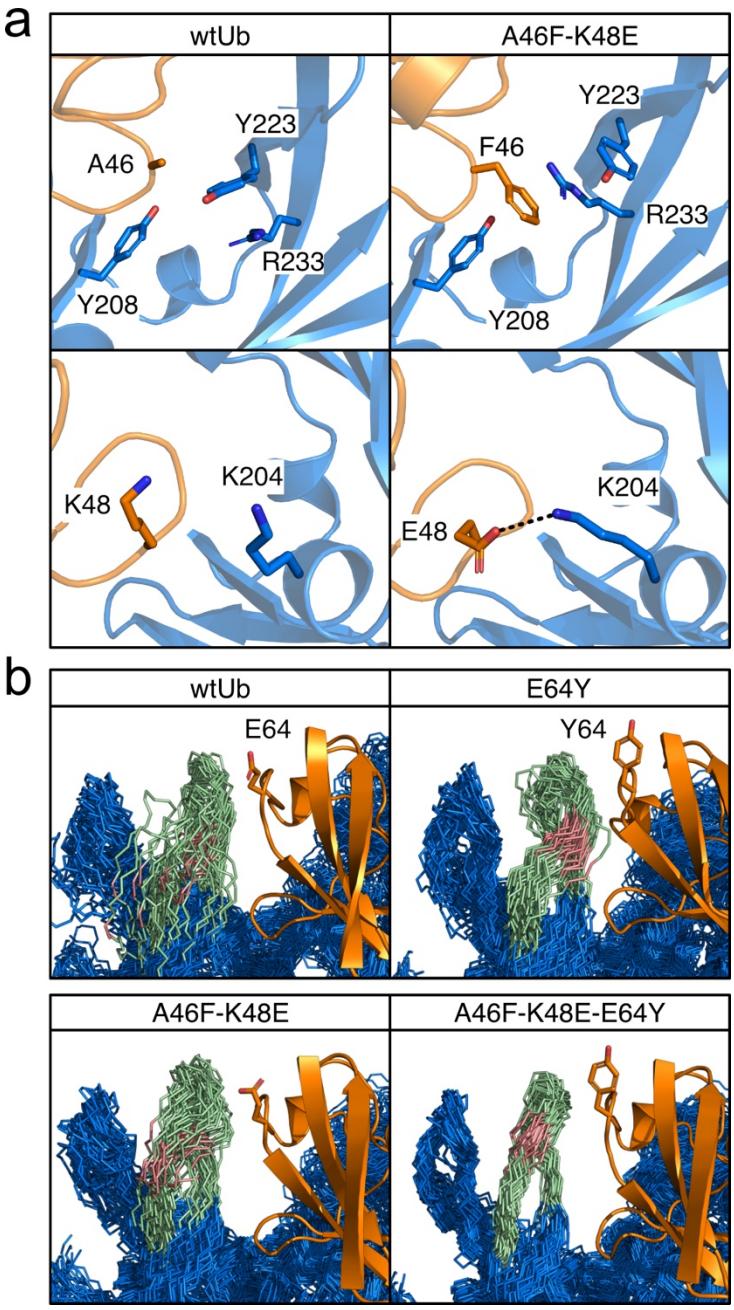

Figure 4. Analysis of conformational dynamics and interactions of wtUb and UbVs for the hydrophobic core and Zn binding region. Ub and PLpro are orange and marine, respectively. **(a)** New attractions introduced by A46F and K48E mutations in the hydrophobic core. **(b)** Superposition of 50 conformations from a 500-ns MD run. The Zn binding region of PLpro (pale green) is highly stabilized by E64Y mutation, where the hinge motion of backbone E230 (salmon) in the interaction network contributes significantly to the loop conformations. Wile-type E64 or mutated Y64 is shown in stick.

References

(1) Swatek, K. N.; Komander, D. Ubiquitin Modifications. *Nature Publishing Group* **2016**, *26*, 399–422. https://doi.org/10.1038/cr.2016.39.

(2) Komander, D.; Rape, M. The Ubiquitin Code. *Annu Rev Biochem* **2012**, *81* (1), 203–229. https://doi.org/10.1146/annurev-biochem-060310-170328.

(3) Kim, W.; Bennett, E. J.; Huttlin, E. L.; Guo, A.; Li, J.; Possemato, A.; Sowa, M. E.; Rad, R.; Rush, J.; Comb, M. J.; Harper, J. W.; Gygi, S. P. Systematic and Quantitative Assessment of the Ubiquitin-Modified Proteome. *Mol Cell* **2011**, *44* (2), 325–340. https://doi.org/10.1016/j.molcel.2011.08.025.

(4) Harrigan, J. A.; Jacq, X.; Martin, N. M.; Jackson, S. P. Deubiquitylating Enzymes and Drug Discovery: Emerging Opportunities. *Nature Reviews Drug Discovery 2017 17:1* **2017**, *17* (1), 57–78. https://doi.org/10.1038/nrd.2017.152.

(5) Morrow, J. K.; Lin, H. K.; Sun, S. C.; Zhang, S. Targeting Ubiquitination for Cancer Therapies. *Future Med Chem* **2015**, *7* (17), 2333. https://doi.org/10.4155/FMC.15.148.

(6) Békés, M.; Rut, W.; Kasperkiewicz, P.; Mulder, M. P. C.; Ovaa, H.; Drag, M.; Lima, C. D.; Huang, T. T. SARS HCoV Papain-like Protease Is a Unique Lys48 Linkage-Specific Di-Distributive Deubiquitinating Enzyme. *Biochemical Journal* **2015**, *468* (2), 215–226. https://doi.org/10.1042/BJ20141170.

(7) Bailey-Elkin, B. A.; Knaap, R. C. M.; Kikkert, M.; Mark, B. L. Structure and Function of Viral Deubiquitinating Enzymes. *J Mol Biol* **2017**, *429* (22), 3441–3470. https://doi.org/10.1016/j.jmb.2017.06.010.

(8) Harcourt, B. H.; Jukneliene, D.; Kanjanahaluethai, A.; Bechill, J.; Severson, K. M.; Smith, C. M.; Rota, P. A.; Baker, S. C. Identification of Severe Acute Respiratory Syndrome Coronavirus Replicase Products and Characterization of Papain-Like Protease Activity. *J Virol* **2004**, *78* (24), 13600–13612. https://doi.org/10.1128/JVI.78.24.13600-13612.2004.

(9) Shin, D.; Mukherjee, R.; Grewe, D.; Bojkova, D.; Baek, K.; Bhattacharya, A.; Schulz, L.; Widera, M.; Mehdipour, A. R.; Tascher, G.; Geurink, P. P.; Wilhelm, A.; van der Heden van Noort, G. J.; Ovaa, H.; Müller, S.; Knobeloch, K.-P.; Rajalingam, K.; Schulman, B. A.; Cinatl, J.; Hummer, G.; Ciesek, S.; Dikic, I. Papain-like Protease Regulates SARS-CoV-2 Viral Spread and Innate Immunity. *Nature* **2020**, *587* (7835), 657–662. https://doi.org/10.1038/s41586-020-2601-5.

(10) Klemm, T.; Ebert, G.; Calleja, D. J.; Allison, C. C.; Richardson, L. W.; Bernardini, J. P.; Lu, B. G.; Kuchel, N. W.; Grohmann, C.; Shibata, Y.; Gan, Z. Y.; Cooney, J. P.; Doerflinger, M.; Au, A. E.; Blackmore, T. R.; Heden van Noort, G. J.; Geurink, P. P.; Ovaa, H.; Newman, J.; Riboldi-Tunnicliffe, A.; Czabotar, P. E.; Mitchell, J. P.; Feltham, R.; Lechtenberg, B. C.; Lowes, K. N.; Dewson, G.; Pellegrini, M.; Lessene, G.; Komander, D. Mechanism and Inhibition of the Papain-like Protease, PLpro, of SARS-CoV-2. *EMBO J* **2020**, *39* (18). https://doi.org/10.15252/embj.2020106275.

(11) Báez-Santos, Y. M.; Mielech, A. M.; Deng, X.; Baker, S.; Mesecar, A. D. Catalytic Function and Substrate Specificity of the Papain-Like Protease Domain of Nsp3 from the Middle East Respiratory Syndrome Coronavirus. *J Virol* **2014**, *88* (21), 12511–12527. https://doi.org/10.1128/JVI.01294-14.

(12) Báez-Santos, Y. M.; St. John, S. E.; Mesecar, A. D. The SARS-Coronavirus Papain-like Protease: Structure, Function and Inhibition by Designed Antiviral Compounds. *Antiviral Res* **2015**, *115*, 21–38. https://doi.org/10.1016/j.antiviral.2014.12.015.

(13) United Nations. *World Economic Situation and Prospects 2022*; New York, 2022.

(14) Bailey-Elkin, B. A.; Knaap, R. C. M.; Johnson, G. G.; Dalebout, T. J.; Ninaber, D. K.; van Kasteren, P. B.; Bredenbeek, P. J.; Snijder, E. J.; Kikkert, M.; Mark, B. L. Crystal Structure of the Middle East Respiratory Syndrome Coronavirus(MERS-CoV) Papain-like Protease Bound to Ubiquitin Facilitates Targeted of Deubiquitinating Activity to Demonstrate Its Role in Innate Immune. *J Biol Chem* **2014**, *289* (50), 34667. https://doi.org/10.1074/JBC.M114.609644.

(15) Lei, J.; Kusov, Y.; Hilgenfeld, R. Nsp3 of Coronaviruses: Structures and Functions of a Large Multi-Domain Protein. *Antiviral Res* **2018**, *149*, 58–74. https://doi.org/10.1016/j.antiviral.2017.11.001.

(16) Shin, D.; Mukherjee, R.; Grewe, D.; Bojkova, D.; Baek, K.; Bhattacharya, A.; Schulz, L.; Widera, M.; Mehdipour, A. R.; Tascher, G.; Geurink, P. P.; Wilhelm, A.; van der Heden van Noort, G. J.; Ovaa, H.; Müller, S.; Knobeloch, K.-P.; Rajalingam, K.; Schulman, B. A.; Cinatl, J.; Hummer, G.; Ciesek, S.; Dikic, I. Papain-like Protease Regulates SARS-CoV-2 Viral Spread and Innate Immunity. *Nature* **2020**, *587* (7835), 657–662. https://doi.org/10.1038/s41586-020-2601-5.

(17) Yang, X.; Chen, X.; Bian, G.; Tu, J.; Xing, Y.; Wang, Y.; Chen, Z. Proteolytic Processing, Deubiquitinase and Interferon Antagonist Activities of Middle East Respiratory Syndrome Coronavirus Papain-like Protease. *Journal of General Virology* **2014**, *95* (PART3), 614–626. https://doi.org/10.1099/VIR.0.059014-0/CITE/REFWORKS.

(18) Osipiuk, J.; Azizi, S.-A.; Dvorkin, S.; Endres, M.; Jedrzejczak, R.; Jones, K. A.; Kang, S.; Kathayat, R. S.; Kim, Y.; Lisnyak, V. G.; Maki, S. L.; Nicolaescu, V.; Taylor, C. A.; Tesar, C.; Zhang, Y.-A.; Zhou, Z.; Randall, G.; Michalska, K.; Snyder, S. A.; Dickinson, B. C.; Joachimiak, A. Structure of Papain-like Protease from SARS-CoV-2 and Its Complexes with Non-Covalent Inhibitors. *Nat Commun* **2021**, *12* (1), 743. https://doi.org/10.1038/s41467-021-21060-3.

(19) Fu, Z.; Huang, B.; Tang, J.; Liu, S.; Liu, M.; Ye, Y.; Liu, Z.; Xiong, Y.; Zhu, W.; Cao, D.; Li, J.; Niu, X.; Zhou, H.; Zhao, Y. J.; Zhang, G.; Huang, H. The Complex Structure of GRL0617 and SARS-CoV-2 PLpro Reveals a Hot Spot for Antiviral Drug Discovery. *Nat Commun* **2021**, *12* (1), 488. https://doi.org/10.1038/s41467-020-20718-8.

(20) Shan, H.; Liu, J.; Shen, J.; Dai, J.; Xu, G.; Lu, K.; Han, C.; Wang, Y.; Xu, X.; Tong, Y.; Xiang, H.; Ai, Z.; Zhuang, G.; Hu, J.; Zhang, Z.; Li, Y.; Pan, L.; Tan, L. Development of Potent and Selective Inhibitors Targeting the Papain-like Protease of SARS-CoV-2. *Cell Chem Biol* **2021**, *28* (6), 855-865.e9. https://doi.org/10.1016/j.chembiol.2021.04.020.

(21) Zhang, W.; Wu, K.-P.; Sartori, M. A.; Kamadurai, H. B.; Ordureau, A.; Jiang, C.; Mercredi, P. Y.; Murchie, R.; Hu, J.; Persaud, A.; Mukherjee, M.; Li, N.; Doye, A.; Walker, J. R.; Sheng, Y.; Hao, Z.; Li, Y.; Brown, K. R.; Lemichez, E.; Chen, J.; Tong, Y.; Harper, J. W.; Moffat, J.; Rotin, D.; Schulman, B. A.; Sidhu, S. S. System-Wide Modulation of HECT E3 Ligases with Selective Ubiquitin Variant Probes. *Mol Cell* **2016**, *62* (1), 121–136. https://doi.org/10.1016/j.molcel.2016.02.005.

(22) van Vliet, V. J. E.; Huynh, N.; Palà, J.; Patel, A.; Singer, A.; Slater, C.; Chung, J.; van Huizen, M.; Teyra, J.; Miersch, S.; Luu, G.-K.; Ye, W.; Sharma, N.; Ganaie, S. S.; Russell, R.; Chen, C.; Maynard, M.; Amarasinghe, G. K.; Mark, B. L.; Kikkert, M.; Sidhu, S. S. Ubiquitin Variants Potently Inhibit SARS-CoV-2 PLpro and Viral Replication via a Novel Site Distal to the Protease Active Site. *PLoS Pathog* **2022**, *18* (12), e1011065. https://doi.org/10.1371/journal.ppat.1011065.

(23) Zhang, Y.; Zhou, L.; Rouge, L.; Phillips, A. H.; Lam, C.; Liu, P.; Sandoval, W.; Helgason, E.; Murray, J. M.; Wertz, I. E.; Corn, J. E. Conformational Stabilization of Ubiquitin Yields Potent and Selective Inhibitors of USP7. *Nature Chemical Biology 2012 9:1* **2012**, *9* (1), 51–58. https://doi.org/10.1038/nchembio.1134.

(24) Sun, M. G. F.; Seo, M. H.; Nim, S.; Corbi-Verge, C.; Kim, P. M. Protein Engineering by Highly Parallel Screening of Computationally Designed Variants. *Sci Adv* **2016**, *2* (7). https://doi.org/10.1126/SCIADV.1600692/SUPPL_FILE/1600692_TABLE_S3.XLSX.

(25) Lee, H.; Lei, H.; Santarsiero, B. D.; Gatuz, J. L.; Cao, S.; Rice, A. J.; Patel, K.; Szypulinski, M. Z.; Ojeda, I.; Ghosh, A. K.; Johnson, M. E. Inhibitor Recognition Specificity of MERS-CoV Papain-like Protease May Differ from That of SARS-CoV. *ACS Chem Biol* **2015**, *10* (6), 1456–1465. https://doi.org/10.1021/cb500917m.

(26) Abraham, M. J.; Murtola, T.; Schulz, R.; Páll, S.; Smith, J. C.; Hess, B.; Lindahl, E. GROMACS: High Performance Molecular Simulations through Multi-Level Parallelism from Laptops to Supercomputers. *SoftwareX* **2015**, *1–2*, 19–25. https://doi.org/10.1016/j.softx.2015.06.001.

(27) Costescu, B. I.; Gräter, F. Time-Resolved Force Distribution Analysis. *BMC Biophys* **2013**, *6* (1), 5. https://doi.org/10.1186/2046-1682-6-5.

(28) Duerksen-Hughes, P. J.; Xu, X.; Wilkinson, K. D. Structure and Function of Ubiquitin: Evidence for Differential Interactions of Arginine-74 with the Activating Enzyme and the Proteases of ATP-Dependent Proteolysis. *Biochemistry* **1987**, *26* (22), 6980–6987. https://doi.org/10.1021/bi00396a019.

(29) Burch, T. J.; Haas, A. L. Site-Directed Mutagenesis of Ubiquitin. Differential Roles for Arginine in the Interaction with Ubiquitin-Activating Enzyme. *Biochemistry* **1994**, *33* (23), 7300–7308. https://doi.org/10.1021/bi00189a035.

(30) Sloper-Mould, K. E.; Jemc, J. C.; Pickart, C. M.; Hicke, L. Distinct Functional Surface Regions on Ubiquitin. *Journal of Biological Chemistry* **2001**, *276* (32), 30483–30489. https://doi.org/10.1074/jbc.M103248200.

(31) Zhang, W.; Bailey-Elkin, B. A.; Knaap, R. C. M.; Khare, B.; Dalebout, T. J.; Johnson, G. G.; van Kasteren, P. B.; McLeish, N. J.; Gu, J.; He, W.; Kikkert, M.; Mark, B. L.; Sidhu, S. S. Potent and Selective Inhibition of Pathogenic Viruses by Engineered Ubiquitin Variants. *PLoS Pathog* **2017**, *13* (5). https://doi.org/10.1371/journal.ppat.1006372.

(32) Wang, J.; Miao, Y. Protein–Protein Interaction-Gaussian Accelerated Molecular Dynamics (PPI-GaMD): Characterization of Protein Binding Thermodynamics and Kinetics. *J Chem Theory Comput* **2022**, *18* (3), 1275–1285. https://doi.org/10.1021/acs.jctc.1c00974.

(33) Wertz, I. E.; Wang, X. From Discovery to Bedside: Targeting the Ubiquitin System. *Cell Chem Biol* **2019**, *26* (2), 156–177. https://doi.org/10.1016/j.chembiol.2018.10.022.

(34) Mevissen, T. E. T.; Komander, D. Mechanisms of Deubiquitinase Specificity and Regulation. *Annu Rev Biochem* **2017**, *86* (1), 159–192. https://doi.org/10.1146/annurev-biochem-061516-044916.